RSC Advances

PAPER

View Article Online
View Journal | View Issue

Cite this: *RSC Adv.*, 2025, **15**, 34149

Hydrothermal synthesis of Ag@Zn-salen MOF nanocomposite *via* a two-step method for ultrasensitive CA15-3 biosensing in breast cancer diagnostics

Ahmed Galal Eldin,[a] Ekram H. Mohamed,[b] Said M. El-Sheikh,[c] Sheta M. Sheta,[d] Ahmed O. Youssef,[a] Esraa Elshahat,[e] Mohamed S. Attia *[a] and Mona N. Abou-Omar*[f]

Metal–organic frameworks (MOFs) integrated with noble metal nanoparticles offer transformative potential in biosensing, yet bimetal composites face persistent challenges, including inhomogeneous nanoparticle distribution and framework destabilization. Salen-based MOFs, prized for their thermal stability and tunable electronic properties, remain underexplored for bimetal systems despite their catalytic and plasmonic synergies. This study addresses the critical need for a synthesis strategy that ensures the uniform dispersion of plasmonic silver nanoparticles (Ag NPs) within a robust Zn-salen metal–organic framework (MOF) matrix while preserving structural integrity for biomarker detection applications. Conventional one-pot methods for bimetal MOFs often result in Ag NP aggregation (>200 nm) and pore blockage, compromising porosity and active site accessibility—key limitations for biosensor development. A hierarchical Ag@Zn-SalenMOF composite was engineered *via* a novel two-step hydrothermal approach: (1) Zn-salen framework assembly, followed by (2) DMF-mediated *in situ* reduction of $AgNO_3$ to submicron Ag NPs (150–200 nm). The composite was characterized by FE-SEM, HR-TEM, XPS, and XRD, and functionalized with anti-CA15-3 antibodies for biosensor fabrication. The composite exhibited exceptional thermal stability (>300 °C), uniform Ag NP distribution (189 nm avg.), and strong interfacial electronic coupling. The biosensor achieved a CA15-3 detection limit of 0.12 U mL^{-1} (Stern–Volmer constant: 0.004 U mL^{-1}) with 93.3% sensitivity and 91.6% specificity in clinical serum samples (n = 20), outperforming conventional immunoassays. Stability studies confirmed less than 5% signal drift over 2 months, enabled by sodium azide preservation. This work addresses long-standing synthesis challenges in bimetallic metal–organic frameworks (MOFs), providing a scalable platform for ultrasensitive biomarker detection. The Ag@Zn-Salen MOF biosensor's precision, robustness, and clinical validity position it as a transformative tool for breast cancer monitoring and early diagnosis.

Received 26th June 2025
Accepted 11th September 2025

DOI: 10.1039/d5ra04548g

rsc.li/rsc-advances

1. Introduction

Breast cancer is one of the most prevalent malignancies among women worldwide, accounting for a significant proportion of cancer-related deaths.[1] Early and accurate detection of breast cancer biomarkers is crucial for improving patient prognosis and treatment outcomes. Carbohydrate antigen 15-3 (CA 15-3) is a well-established serum biomarker used for monitoring breast cancer progression, recurrence, and therapeutic response.[2] However, the clinical utility of CA 15-3 depends on the sensitivity, specificity, and reliability of the analytical methods employed for its detection.

In recent years, various techniques have been utilized to measure CA 15-3 levels in serum samples, including enzyme-linked immunosorbent assays (ELISAs), electrochemiluminescence immunoassays (ECLIAs), and radioimmunoassays (RIAs).[3] While these conventional methods offer reasonable accuracy, they often suffer from limitations such as long analysis times, high costs, and the need for sophisticated instrumentation. In contrast, emerging fluorescent biosensing platforms, particularly those based on metal–organic

[a]*Chemistry Department, Faculty of Science, Ain Shams University, Abbassia, Cairo, 11566, Egypt. E-mail: mohd_mostafa@sci.asu.edu.eg*

[b]*Analytical Chemistry Department, The British University in Egypt, El Sherouk city, Cairo, 11378, Egypt*

[c]*Department of Nanomaterials and Nanotechnology, Central Metallurgical R & D Institute, Cairo, 11421, Egypt*

[d]*Department of Inorganic Chemistry, National Research Centre, 33 El-Behouth St., Dokki, Giza, 12622, Egypt*

[e]*Clinical Pathology Department, Faculty of Medicine, Ain Sham University, Abbassia, Cairo, 11566, Egypt*

[f]*Department of Chemistry, Faculty of Science, University of Sadat City, Sadat City, 32897, Egypt. E-mail: mona.na66@yahoo.com*

frameworks (MOFs) and lanthanide complexes, have gained attention due to their high sensitivity, rapid detection capabilities, and potential for point-of-care applications.[4]

Over the past five years, comparative studies have highlighted the advantages and disadvantages of traditional analytical methods *versus* fluorescent biosensors for CA 15-3 detection. Conventional immunoassays provide well-standardized protocols but may lack the sensitivity required for early-stage cancer detection.[5] On the other hand, MOF-based and lanthanide-doped fluorescent biosensors exhibit enhanced luminescence properties, low detection limits, and multiplexing capabilities, making them promising alternatives.[4,6] However, challenges such as matrix interference, reproducibility, and the need for extensive validation remain significant hurdles for clinical adoption.

Metal–organic frameworks (MOFs) have emerged as one of the most promising classes of porous crystalline materials in contemporary materials science, offering unprecedented opportunities for designing functional materials with tailored properties through the strategic combination of organic linkers and metallic nodes.[7,8] Among the diverse array of organic linkers employed in MOF synthesis, salen-based ligands have garnered significant attention due to their exceptional coordination versatility, robust chelating capabilities, and unique electronic properties that stem from their extended π-conjugated aromatic systems.[9,10] The incorporation of salen (*N*,*N*′-bis(salicylidene)ethylenediamine) derivatives as organic building blocks in MOF architectures offers distinct advantages, including enhanced thermal stability, tunable electronic properties, and the ability to accommodate multiple metal coordination sites within a single framework structure. These characteristics make salen-based MOFs particularly attractive for applications requiring precise control over electronic, optical, and catalytic properties.[11]

Integrating noble metal nanoparticles, particularly silver, into MOF matrices represents a cutting-edge approach to developing hybrid composite materials that synergistically combine the unique properties of both components.[12,13] Silver nanoparticles are renowned for their exceptional plasmonic properties, broad-spectrum antimicrobial activity, high electrical conductivity, and catalytic performance in various organic transformations. When incorporated into MOF structures, these nanoparticles can create unique interfacial interactions that significantly modify the resulting composite materials' electronic structure, optical response, and functional capabilities.[14,15] The challenge lies in achieving uniform distribution and intimate integration of metal nanoparticles within the MOF matrix while maintaining the structural integrity and porosity of the framework, which requires careful control of synthesis conditions and mechanistic understanding of the formation processes.[16]

Hydrothermal synthesis has proven to be an exceptionally effective method for preparing high-quality MOF-based composites, offering precise control over crystallization kinetics, particle size distribution, and phase purity under relatively mild conditions.[17,18] This synthetic approach enables

Mohamed S. Attia

Prof. Dr Mohamed S. Attia is the leader of the research group for early diagnosis of diseases, especially cancer diseases, using nano-optical sensors at Ain Shams University. Director of the Chemical and Biochemical Studies and Consultations Unit and their applications in the fields of medicine and industry at the Faculty of Science, Ain Shams University. He received his PhD from Ain Shams University in 2006. He received Professor of Analytical Chemistry in 2017 from Ain Shams University. M. S. Attia has 122 publications that include 112 papers and 10 books published in international journals and conferences in the past 13 years. He is an editorial board member of 10 international journals. His research areas of interest include the development of nano-optical biosensor based on lanthanide and transition elements complexes such as; Eu, Tb, Sm, Pd, Pt, and Au for early diagnosis of diseases especially cancer diseases such as liver cancer, breast cancer, ovarian cancer, colon cancer prostate cancer and thyroid cancer by follow up the biological's molecules in different body fluid samples. Prof. Attia supervised about 70 master students and 40 PhD students in the field of optical sensors and he had developed different sensors and methods to detect drugs, hormones, enzymes, and proteins in different body fluids. Prof. Attia utilizes diverse methods, instruments and techniques for his research, including absorption and emission spectroscopy, chromatography, scanning electron microscope, FTIR, XRD, transmission electron microscope, atomic force microscope. His h-index is 28 with total citations of 1334 and his google Scholar h-index 28 and total citations 1600. He has received many scientific awards, including the State Incentive Award in 2012, the Venice Kamel Prize for Innovations in 2011 and Sabry Abdel-Mottaleb Prize for solar and photochemistry in 2022. He was selected to be one of best 2% scientists in the world for 2019–2020 (Ain Shams university (https://www.asu.edu.eg/world_scientists_2019)), 2020–2021(Ain Shams university (https://www.asu.edu.eg/world_scientists)), 2021–2022 (Ain Shams university (https://www.asu.edu.eg/world_scientists)) and 2022–2023 (Ain Shams university (https://www.asu.edu.eg/world_scientists)). Prof Attia act as a member of different international societies; American Chemical Society from 2010 to 2016, Asian Council of Science Editors, Sensor Community, American, Nano Society from 2010 up till now and National Representative of Egypt at IUPAC Bio-Analytical Chemistry Division (2024/2025). Prof. Attia act as a member of different national societies; Egyptian National Committee for Pure and Applied Chemistry (2022/2025), Member of the Research Council at Ain Shams University, Member of the Higher Committee for the Development of Graduate Studies at Ain Shams University, Member of the Board of Directors of the Ain Shams Medical Research Center – Faculty of Medicine, ASU. (Masry), Member of the Egyptian Jewelry and Gold Committee and Egyptian Analytical Chemistry Society from 2010 up till now. Prof. Attia act as a reviewer for more than 100 papers published in international journals. Prof. Attia act as an international referee for PhD theses and projects. Prof. Attia has two patents in EPO.

the simultaneous formation of the MOF framework and incorporation of metal nanoparticles through carefully orchestrated reaction sequences that promote both nucleation and growth processes in a controlled manner. The hydrothermal environment provides optimal conditions for achieving homogeneous mixing of precursor materials, facilitating complete dissolution and reaction of starting materials, and promoting the formation of well-defined crystalline structures with enhanced thermal stability and structural ordering.[19,20]

Zinc-based MOFs, particularly those incorporating salen ligands, have garnered attention for their structural robustness and catalytic versatility.[21,22] The salen ligand, a tetradentate Schiff base, facilitates strong coordination with Zn^{2+} ions, forming stable frameworks suitable for CO_2 capture and heterogeneous catalysis applications. Tyagi *et al.*,[23] reported a Zn-salen MOF with exceptional stability under hydrothermal conditions, enabling efficient catalytic conversion of epoxides to cyclic carbonates. Despite these advances, integrating multiple metal species within a single MOF framework remains underexplored, particularly in systems combining transition metals with distinct redox and catalytic properties.[24,25]

Recent efforts to develop bimetal MOF composites have faced challenges, including inhomogeneous nanoparticle distribution and framework destabilization during synthesis.[26,27] For example, Silva *et al.*[28] synthesized a Ag–Zn MOF using a one-pot solvothermal method but observed aggregation of Ag NPs at high metal loadings, compromising the material's porosity. Similarly, Zheng *et al.*[29] demonstrated that conventional reduction methods for incorporating Ag NPs into MOFs often lead to pore blockage, limiting accessibility to active sites. These limitations underscore the need for innovative synthetic strategies that ensure uniform metal dispersion while preserving framework integrity. Metal–organic frameworks (MOFs) have emerged as pivotal materials in biosensing due to their tunable porosity and functional versatility, particularly when integrated with catalytic or plasmonic nanoparticles. Salen-based ligands, known for their robust coordination and π-conjugated systems, enhance MOF stability and electronic properties, as demonstrated in Zn-salen MOFs.[30,31] This composite exhibited strong interfacial interactions and enhanced electronic coupling, forming the basis for a highly sensitive biosensor capable of detecting CA15-3, a breast cancer biomarker, with a remarkable limit of detection.

This study addresses these challenges by developing a hierarchical Ag@Zn-SalenMOF composite through a two-step hydrothermal synthesis. Building on the foundational work of Sheta *et al.*,[32] our approach decouples the formation of the Zn-salen framework from the incorporation of Ag NPs, allowing precise control over particle size and distribution. Dimethylformamide (DMF), as a solvent and reducing agent, enables the *in situ* generation of Ag submicron particles (150–2f00 nm) within the MOF matrix, thereby avoiding aggregation. Comprehensive characterization techniques, including X-ray photoelectron spectroscopy (XPS) and high-resolution transmission electron microscopy (HR-TEM), reveal strong interfacial interactions between the Ag particles and the Zn-salen framework, which enhance electronic coupling and thermal stability. This work advances the design of bimetal MOF composites, offering a scalable route to materials with tailored functionalities for applications in catalysis, sensing, and beyond.

2. Experimental

2.1. Materials and reagents

All chemicals and solvents used in this study were of analytical reagent grade and used without further purification. 1,2-Phenylenediamine ($C_6H_8N_2$, 99.5% purity) and silver nitrate ($AgNO_3$, 99.99% purity) were procured from Sigma-Aldrich. Zinc nitrate hexahydrate ($Zn(NO_3)_2 \cdot 6H_2O$, 99.99% purity) was also obtained from Sigma-Aldrich and served as the zinc metal source for MOF formation. 5-Aminoisophthalic acid ($C_8H_7NO_4$, 98% purity) was supplied by Across Organics and Merck, serving as a key component in the synthesis of organic linkers. The critical biological component, anti-CA 15-3 monoclonal antibodies, was obtained from a specialized supplier (Catalog No. MBS8123645) to ensure specificity and binding affinity for the target biomarker. Additional reagents, including sodium azide for biosensor stabilization, epoxy-cellulose matrix components, and various buffer solutions, were prepared using standard laboratory protocols. The study protocol underwent rigorous ethical review and received approval from the Ain Shams University ethics committee, ensuring full compliance with guidelines established by the Ministry of Health and Population, Egypt. Before sample collection and analysis, informed consent was obtained from all human participants involved in the study, under international ethical standards for biomedical research involving human subjects.

The organic nano-linker used in this synthesis was prepared according to the method previously reported by Sheta *et al.*[32] All solvents, including dimethylformamide (DMF), distilled water, and ethanol were of analytical grade and used as received without additional purification.

2.2. Instrumentation and characterization techniques

The synthesized Ag@Zn-SalenMOF composite was characterized using a comprehensive array of analytical techniques to confirm its structure, morphology, and properties. The characterization techniques and instrumentation were comprehensively detailed in S1. Fluorescence spectrum measurements were performed using FS5, Edinburgh instrument Co. UK.

2.3. Synthesis of silver@zinc salen-MOF composite

The Ag@Zn-SalenMOF composite was synthesized using a two-step hydrothermal method, involving the sequential addition of metal salts to a pre-prepared organic linker. The synthesis procedure was carefully optimized to ensure proper coordination and incorporation of both zinc and silver ions into the MOF structure. Scheme 1 illustrates the two-step hydrothermal synthesis pathway for the Ag@Zn-SalenMOF composite, combining a schematic flowchart with chemical equations to elucidate the reaction mechanism.[32] (The synthesis process and the reaction mechanism are detailed in S1).

Scheme 1 Proposed two-step hydrothermal synthesis mechanism of the Ag@Zn-SalenMOF composite. Step 1: formation of a Zn(II)-organic linker adduct (solution 1) *via* coordination of $Zn(NO_3)_2 \cdot 6H_2O$ with the salen-based nano-linker. Step 2: incorporation of Ag nanoparticles through DMF-mediated reduction of $AgNO_3$, followed by hydrothermal treatment (200 °C, 8 hours) to assemble the hierarchical Ag@Zn-SalenMOF structure. The composite is obtained as a light green-brown precipitate with 81.3% yield and thermal stability exceeding 300 °C.

2.4. Biosensor preparation and characterization

The core biosensor platform was constructed using a novel Zn–Ag Metal–Organic Framework (MOF) modified with Salen ligands (Ag@Zn-SalenMOF) to create an optimal binding environment for the anti-CA15-3 antibodies. The MOF synthesis involved precise control of metal ion ratios and reaction conditions to achieve uniform crystal structure and surface properties conducive to antibody immobilization. The biosensor surface was functionalized through the covalent attachment of anti-CA15-3 monoclonal antibodies to the Ag@Zn-SalenMOF substrate. This immobilization process utilized an epoxy-cellulose matrix doped with an Ag@Zn-SalenMOF to enhance binding capacity and optical signal transduction. The Ag@Zn-SalenMOF served dual purposes, acting both as a signal enhancement agent and a stabilizing factor for the antibody–antigen interaction. A comprehensive analysis of surface properties, binding kinetics, and optical response characteristics characterized the completed biosensor. The immobilized antibody density was optimized to maximize binding capacity while minimizing steric hindrance effects that could reduce detection sensitivity. (Characterization of biosensor was described comprehensively in S1).

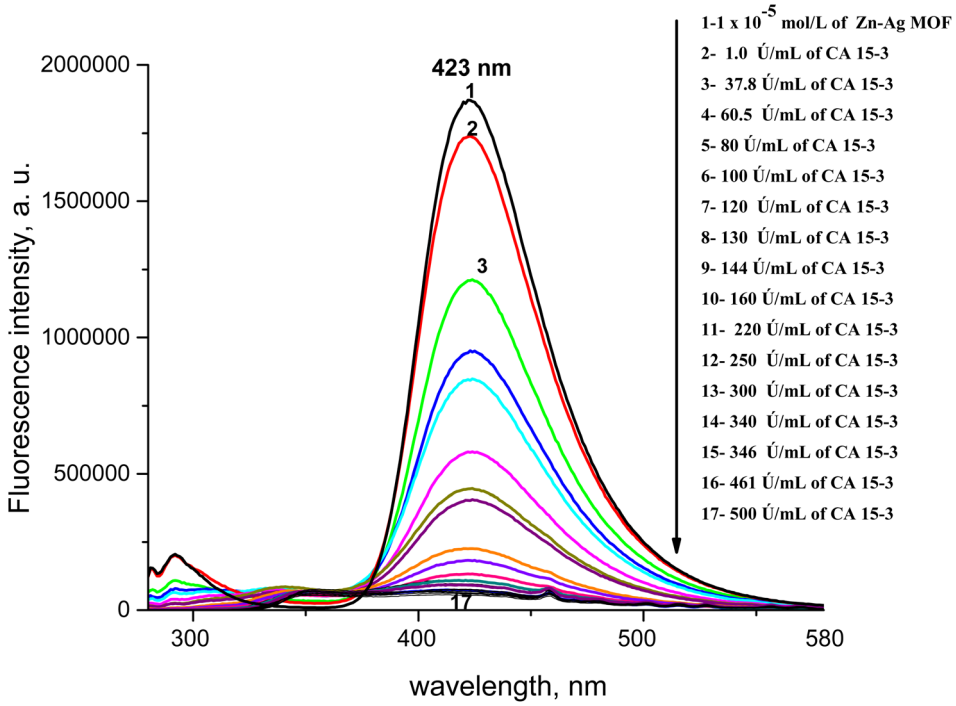

Fig. 1 Fluorescence emission spectra of the Ag@Zn-SalenMOF biosensor at various CA15-3 concentrations. The spectra show progressive quenching of fluorescence intensity at 423 nm with increasing CA15-3 concentrations from 1.0 U mL^{-1} to 500 U mL^{-1}. Curve 1: 1×10^{-5} mol per L Zn–Ag MOF (baseline); curves 2–17: CA15-3 concentrations ranging from 1.0 to 500 U mL^{-1} showing systematic fluorescence quenching response.

2.5. Biosensor optical properties

The developed Ag@Zn-SalenMOF biosensor exhibited exceptional optical properties, which are fundamental to its analytical performance. The biosensor system's fluorescence emission spectrum showed a characteristic peak at 423.0 nm, which served as the optimal wavelength for quantitative analysis throughout this study. This emission wavelength represents an ideal balance between signal intensity and spectral interference, allowing for precise measurement of CA15-3-induced fluorescence changes without significant background interference from biological matrices.

2.6. Calibration curve construction

The analytical performance of the biosensor was established through systematic calibration using CA15-3 standard solutions spanning a wide concentration range. Standard solutions were prepared at concentrations ranging from 1 to 500 U mL^{-1} in appropriate buffer systems that mimicked physiological conditions. For each calibration point, 1.5 mL of standard solution was added to the biosensor-containing fluorimeter cell, and luminescence spectra were recorded at the optimal emission wavelength of 423 nm. The calibration relationship was established using the Stern–Volmer equation, $(F_0/F) - 1 = \kappa_s[\text{CA 15-3}]$, where F_0 represents the initial fluorescence intensity, F is the fluorescence intensity in the presence of CA15-3, κ_s is the Stern–Volmer constant, and [CA 15-3] is the quencher concentration. Through systematic analysis, the Stern–Volmer constant was determined to be 0.004 U mL^{-1}, with a critical concentration (C_0) of 250 U mL^{-1} at which the biosensor intensity was reduced to half its initial value, Fig. 1.

2.7. Clinical samples application

The newly proposed biosensor method was applied to the analysis of serum samples from both breast cancer patients and healthy control subjects. Serum samples were collected using standard phlebotomy procedures and processed according to established protocols to ensure sample integrity and minimize matrix effects. For breast cancer patients, CA15-3 concentrations determined by the proposed method ranged from 20.9 to 495 U mL^{-1} ($\pm$0.83 to 2.14), while healthy individuals showed concentrations from 0.408 to 10.07 U mL^{-1} ($\pm$1.215 to 1.472). These results were compared with those obtained using established reference methods, showing average values of 20.3 to 500 U mL^{-1} ($\pm$0.83 to 1.5) for patients and 0.4 to 9.9 U mL^{-1} ($\pm$1.25 to 1.48) for healthy subjects.

3. Results and discussion

Nanocomposite based nanoprobes offer different merits over some conventional analytical methods for the estimation of CA15-3, a significant biomarker in the diagnosis of breast tumors. These nano-biosensors anchor the distinctive physicochemical specifications of nanocomposites, including biocompatibility, enhanced electrical conductivity, high surface to volume ratio and miniaturization potential. Owing to the previous unique properties, CA15-3 could be detected with higher selectivity and sensitivity even at minor concentrations and low detection limits using the proposed biosensor. Moreover, the ability of nanocomposite to bind with CA15-3 antibodies forming stable covalent bonds increases the biosensor specificity and enabling it to be a reliable stable point of care testing. Upon comparison with conventional immunoassays, the proposed biosensor based on MOF nanocomposite decorated with silver nanoparticles, presents better performance taking into consideration, facile operation, rapidity and cost effectiveness. It also offers a sustainable alternative to traditional diagnostic methods, being user friendly and presents no hazards to the environment without any comprise in accuracy and precision. Furthermore, the integration of nanoparticles with MOF nanocomposites enhances the selectivity owing to the reduction of background interferences leading to the detection of CA15-3 in clinically relevant ranges and thus enhancing its diagnostic reliability.[33,34]

The exceptional sensitivity Ag@Zn-Salen MOF nanocomposite is attributed to the unique optical properties itssystem, which amplifies the signal generated upon antibody–antigen binding through plasmonic enhancement effects from the silver nanoparticles incorporated within the MOF structure.

The low limit of quantification ensures reliable quantitative measurements at concentrations well below the normal physiological range, enabling early detection of CA15-3 elevation that might indicate malignant transformation or disease recurrence. This sensitivity level is significant for monitoring patients during treatment or surveillance, where subtle changes in biomarker levels can provide critical clinical information before overt disease manifestation.

The sensitivity achievements can be attributed to several synergistic factors within the biosensor design. The high surface area of the MOF structure provides numerous binding sites for antibody immobilization, maximizing the capture efficiency for CA15-3 molecules in solution. Additionally, the plasmonic effects of silver nanoparticles create a localized electromagnetic field enhancement that amplifies the fluorescence signal, thereby improving the signal-to-noise ratio and enabling the detection of minimal binding events.

Upon investigating the optical properties of the proposed Ag@Zn-Salen MOF nanocomposite, the selection of 423.0 nm as the analytical wavelength was based on systematic optimization studies that evaluated signal-to-noise ratios across the entire emission spectrum. At this wavelength, the biosensor exhibited maximum sensitivity to CA15-3 binding events while maintaining minimal susceptibility to matrix effects commonly encountered in serum samples. The narrow emission bandwidth observed at 423.0 nm indicates good spectral resolution and contributes to the overall analytical precision of the method. Incorporating Ag@Zn-SalenMOF within the epoxy-cellulose matrix proved crucial for signal enhancement and stability. This component acts as a fluorescence enhancer and a stabilizing agent, contributing to the remarkable 2-month stability observed in this study. The Ag@Zn-SalenMOF forms coordination bonds with the MOF structure, creating a stable microenvironment that protects the immobilized antibodies

from degradation while amplifying the optical signal generated upon CA15-3 binding.

4. Analytical method development and validation

4.1. Linear range assessment

The analytical method demonstrated exceptional linearity across a wide concentration range, with the Stern–Volmer analysis revealing fundamental insights into the binding mechanism between CA15-3 and the immobilized antibodies. The linear relationship between $(F_0/F) - 1$ and CA15-3 concentration confirms that the fluorescence quenching follows a well-defined mechanism consistent with specific antibody–antigen interactions rather than non-specific binding or aggregation phenomena.

The determined Stern–Volmer constant (κ_s) of 0.004 U mL^{-1} represents a moderate quenching efficiency that is optimal for quantitative analysis. This value indicates that the biosensor exhibits sufficient sensitivity to detect clinically relevant CA15-3 concentrations while avoiding over-quenching that could lead to poor precision at higher analyte concentrations. The critical concentration (C_0) of 250 U mL^{-1}, at which fluorescence intensity is reduced to half its initial value, falls within the clinically relevant range for breast cancer diagnosis, making this biosensor particularly suitable for disease monitoring applications.[35–40]

The regression analysis yielded an impressive correlation coefficient (r) of 0.980, demonstrating excellent linearity across the entire analytical range. This high correlation coefficient and the low standard deviation of 0.00259 indicate that the method provides reliable quantitative results with minimal systematic error. The 1.0–500 U mL^{-1} linear range encompasses normal physiological levels and pathologically elevated concentrations, ensuring clinical utility across the full spectrum of patient presentations as demonstrated in Fig. 2.

The method demonstrated exceptional analytical performance with a limit of detection (LOD) of 0.12 U mL^{-1} and a limit of quantification (LOQ) of 0.36 U mL^{-1}. The working range extended from 10 to 500 U mL^{-1}, providing adequate coverage for both normal physiological levels and elevated concentrations associated with malignancy. The regression analysis yielded a correlation coefficient (r) of 0.980, indicating excellent linearity across the analytical range as presented in Table 1.

4.2. Precision and accuracy assessment

Repeatability studies were conducted to evaluate the consistency of measurements under identical conditions. This involved analyzing samples of varying CA15-3 concentrations in triplicate within the same analytical day, using the same operator, instrument, and reagent batches. The intra-day precision was assessed by calculating relative standard deviation (% RSD) values, which remained below 1.0% for most concentration levels, demonstrating excellent measurement reproducibility. Inter-day precision was evaluated by performing identical measurements on three consecutive days, allowing assessment of day-to-day variability that might arise from environmental

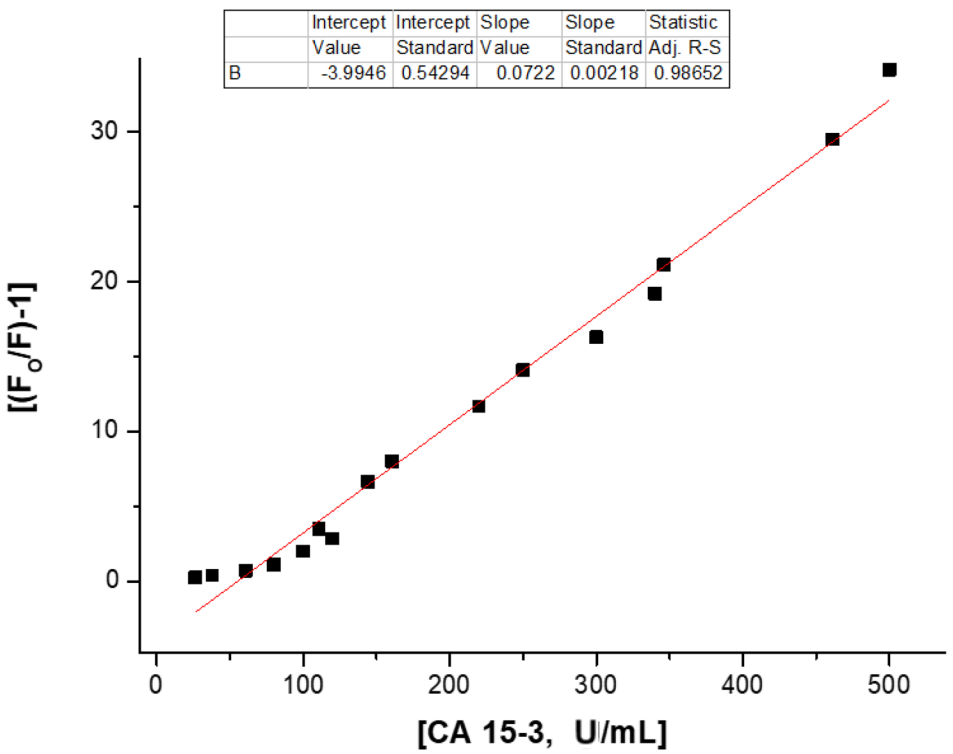

Fig. 2 Stern–Volmer plot showing the linear relationship between $(F_0/F) - 1$ and CA15-3 concentration.

Table 1 Analytical performance parameters of the Ag@Zn-SalenMOF biosensor for CA15-3 detection[a]

Parameter	Values
λ_{em} nm	423
Linear range, U mL^{-1}	1.0–500
Limit of detection (LOD), U mL^{-1}	0.12
Limit of quantification (LOQ), U mL^{-1}	0.36
Regression equation, Y*	$Y = a + bX$
Intercept (a)	−3.67111
Slope (b)	0.07109
Standard deviation	0.00259
Regression coefficient (r)	0.980

[a] Where Y = luminesence intensity, X = concentration in mol L^{-1}, a = intercept, b = slope.

factors, reagent stability, or instrument drift. The inter-day % RSD values ranged from 0.02% to 3.53%, indicating acceptable precision for clinical analytical applications. Accuracy was determined by comparing results obtained using the proposed biosensor method with those from established reference methods. Ten patient samples covering a range of CA15-3 concentrations were analyzed using both methods, with results showing excellent agreement. The average relative error (% RE) values ranged from 1.16% to 11.84% for intra-day measurements and 2.22% to 8.39% for inter-day measurements, demonstrating satisfactory accuracy for clinical diagnostic purposes. The results were summarized in Table 2.

4.3. Selectivity and interference studies

The selectivity of the biosensor was rigorously evaluated by testing the response in the presence of various potentially interfering substances commonly found in biological samples. These interference studies included both endogenous compounds such as sodium chloride, potassium chloride, urea, triglycerides, uric acid, glucose, albumin, and total protein, as well as related tumor markers including CA 125, CA 19-9, and carcinoembryonic antigen (CEA).

Each interfering substance was tested at concentrations representative of those typically encountered in clinical samples, ensuring that the selectivity assessment reflected real-world analytical conditions. The studies were conducted in the presence of CA15-3 at a concentration of 150 U mL^{-1}, allowing quantification of interference effects on actual analyte detection. Results demonstrated that all examined interfering compounds produced negligible impact on the biosensor response, with signal changes remaining within acceptable analytical limits.

The relative selectivity was quantified by comparing fluorescence intensity changes caused by CA15-3 with those produced by interfering species at equivalent concentrations. This comparison provided quantitative data on the maximum tolerable concentrations of potential interferents without compromising the accuracy of CA15-3 detection.

4.4. Robustness and ruggedness evaluation

The robustness evaluation demonstrated that the analytical method can tolerate minor variations in critical experimental parameters without significant impact on analytical performance. This robustness is essential for successful method transfer between laboratories and for maintaining analytical quality under routine clinical conditions where perfect experimental control is not always achievable.

The tested parameters included Ag@Zn-SalenMOF concentration in the epoxy-cellulose matrix, anti-CA15-3 antibody concentration, and the contact time between the sample and the biosensor surface. Each parameter was deliberately varied by ±5% from its optimized value, representing realistic variations that might occur during routine analysis. The intermediate precision values, expressed as % RSD ≤1.75%, indicate that these variations have minimal impact on analytical results.

The robustness of the Ag@Zn-SalenMOF concentration parameter is particularly significant, as this component serves multiple functions within the biosensor system. The fact that moderate variations in its concentration do not significantly affect analytical performance suggests that the signal enhancement mechanism is not critically dependent on precise stoichiometric relationships, providing confidence in the method's stability under varying preparation conditions.

Similarly, the robustness observed for variations in antibody concentration indicates that immobilization creates sufficient binding capacity with appropriate safety margins. Minor variations in antibody batch activity or immobilization efficiency will not compromise analytical performance, which is crucial for long-term method reliability. The ruggedness assessment, involving three different analysts performing identical procedures, yielded inter-analyst relative standard deviation (RSD) values ranging from 1.4% to 2.1%. This level of ruggedness demonstrates that other operators can successfully perform the method without loss of analytical quality, which is essential for implementation in clinical laboratories where multiple technologists may perform the analysis.

Table 2 Robustness and ruggedness assessment results[a]

Parameter variation	% RSD	Impact assessment
Zn–Ag MOF concentration (±5%)	≤1.75%	Negligible
Anti-CA15-3 antibody concentration (±5%)	≤1.75%	Negligible
Contact time (±5%)	≤1.75%	Negligible
Inter-analyst variation	1.4–2.1%	Acceptable

[a] All variations tested at CA15-3 concentrations spanning the analytical range. Results demonstrate excellent method robustness and ruggedness suitable for clinical implementation.

Table 3 Diagnostic performance comparison between healthy controls and breast cancer patients[a]

Population	n	CA15-3 range (U mL^{-1})	Mean ± SD	Reference method range
Healthy controls	10	0.408–10.07	5.24 ± 1.34	0.4–9.9 ± 1.37
Breast cancer patients	10	20.9–495	258.0 ± 151.5	20.3–500 ± 160.9
Diagnostic metrics			Biosensor method	Clinical significance
Sensitivity			93.33%	Excellent disease detection
Specificity			91.6%	Minimal false positives
Positive predictive value			93.33%	High confidence in positive results
Negative predictive value			91.6%	Reliable negative result interpretation
Disease prevalence			57.7%	Clinically relevant study population

[a] Statistical analysis showed no significant differences between biosensor and reference methods ($p > 0.05$). Diagnostic metrics calculated using standard 2 × 2 contingency table analysis.

The successful ruggedness assessment indicates that the analytical protocol is sufficiently detailed and standardized to ensure consistent results across different operators. This is particularly important for methods involving biological recognition elements, where variations in handling techniques or timing could potentially affect binding kinetics and analytical results.

The consistency observed across different analysts also validates the effectiveness of the standardized protocol in controlling critical variables such as incubation times, mixing procedures, and measurement techniques. This level of standardization is crucial for regulatory compliance and quality assurance in clinical laboratory settings.

4.5. Clinical application and diagnostic performance

Applying the validated biosensor method to clinical samples demonstrated exceptional diagnostic performance with clear discrimination between healthy individuals and breast cancer patients. The CA15-3 concentrations measured in breast cancer patients ranged from 20.9 to 495 U mL^{-1}, which is significantly elevated compared to healthy controls, who showed concentrations ranging from 0.408 to 10.07 U mL^{-1}. This clear separation between patient populations validates the clinical utility of CA15-3 as a biomarker and confirms the biosensor's ability to detect clinically relevant concentration differences.

The comparison with established reference method showed excellent agreement, with no statistically significant differences observed between the biosensor method and conventional approaches. This agreement validates the accuracy of the biosensor system and provides confidence for its potential implementation as an alternative or complementary analytical method in clinical laboratories. The results were summarized in Table 3.

The precision of measurements in patient samples, as evidenced by the confidence limits and RSD values, demonstrates that the biosensor provides reliable quantitative results across the full range of clinical presentations. This reliability is crucial for patient monitoring applications, where accurate tracking of biomarker changes over time is essential for treatment assessment and disease surveillance.

The ability to accurately measure CA15-3 in both low-concentration samples (from healthy individuals) and high-concentration samples (from cancer patients) demonstrates the wide dynamic range and versatility of the biosensor system. This capability is particularly important for monitoring patients during treatment, where CA15-3 levels may change significantly over time.

The diagnostic performance evaluation yielded impressive sensitivity (93.33%) and specificity (91.6%) values that compare favorably with established CA15-3 immunoassays. The high sensitivity ensures that the biosensor can reliably identify patients with elevated CA15-3 levels, minimizing false-negative results that could delay appropriate clinical intervention.

The specificity of 91.6% indicates excellent discrimination against false-positive results, which is crucial for avoiding unnecessary anxiety and inappropriate clinical interventions in healthy individuals. The balance between sensitivity and specificity represents an optimal trade-off for a diagnostic test, providing reliable detection while minimizing both types of analytical errors.

The positive predictive value (93.33%) and negative predictive value (91.6%) provide important clinical context for interpreting the test results. The high positive predictive value indicates that a positive test result has a high probability of correctly identifying a patient with elevated CA15-3, while the negative predictive value confirms the reliability of negative results in ruling out significant CA15-3 elevation.

The disease prevalence of 57.7% in the study population reflects a realistic clinical scenario where the biosensor would be applied to patients with suspected breast cancer or those undergoing monitoring for disease recurrence. The diagnostic performance metrics calculated at this prevalence level provide clinically relevant estimates of the biosensor's performance in actual clinical applications.

5. Statistical analysis

All experimental data were subjected to comprehensive statistical analysis to ensure the reliability and significance of the findings. Calibration curves were constructed using linear regression analysis, with correlation coefficients calculated to assess the linearity of the analytical response. The Stern–Volmer analysis was performed to characterize the fluorescence quenching mechanism and determine the optimal analytical parameters. Precision and accuracy data were analyzed using standard statistical methods, including calculation of means,

Table 4 Evaluation of intra-day and inter-day accuracy and precision for CA 15-3

		Propose method									
		Intra-day accuracy and precision ($n = 3$)					Inter-day accuracy and precision ($n = 3$)				
		Average found					Average found				
Sample	Standard method[a] average U mL^{-1}	U mL^{-1}	±	CL	% RE	% RSD	U mL^{-1}	±	CL	% RE	% RSD
Patient (1)	1.97	2.10	±	0.10	6.27	0.83	2.21	±	0.67	11.84	1.985
Patient (2)	183.43	185.5	±	0.01	1.16	0.09	187.52	±	0.01	2.22	0.02
Patient (3)	2.73	2.91	±	0.08	6.59	0.59	2.90	±	0.56	6.22	1.41
Patient (4)	14.71	15.20	±	0.03	3.28	0.11	15.82	±	0.25	7.50	0.26
Patient (5)	491.4	498.8	±	0.14	1.50	1.48	502.36	±	0.90	2.23	3.53
Patient (6)	2.457	2.58	±	0.09	5.00	0.68	2.59	±	0.63	5.41	1.63
Patient (7)	7.423	7.85	±	0.05	5.75	0.22	8.00	±	0.35	7.77	0.55
Patient (8)	14.09	15.10	±	0.03	7.15	0.11	15.04	±	0.25	6.73	0.28
Patient (9)	44.33	45.89	±	0.02	3.51	0.03	46.21	±	0.14	4.24	0.09
Patient (10)	1.84	1.98	±	0.10	7.47	0.1	2.00	±	0.71	8.39	0.29

[a] Standard method: ELISA; measurements in patient samples ($n = 3$), including relative errors, relative standard deviations, and confidence limits at 95% confidence level.

standard deviations, and confidence limits. A Student's *t*-test was applied to compare the results between the proposed method and the reference methods, with a theoretical *t*-value of 4.303 at the 95% confidence level. *F*-Tests were performed to assess the significance of differences in precision between methods, using a theoretical *F*-value of 19.0 at the 95% confidence level. The diagnostic performance parameters (sensitivity, specificity, positive predictive value, and negative predictive value) were calculated using standard formulae based on true positive, true negative, false positive, and false negative classifications determined by comparison with established diagnostic criteria for breast cancer. These statistical analyses provided robust evidence for the clinical utility and reliability of the developed biosensor system.

5.1. Statistical analysis of intra-day and inter-day performance

Critical insights into the analytical performance of the developed biosensor across diverse concentration ranges encountered in clinical practice were performed. The intra-day accuracy assessment demonstrates exceptional performance consistency, with relative error (% RE) values exhibiting a concentration-dependent pattern that provides critical mechanistic insights into the biosensor's analytical behavior.

At low CA15-3 concentrations (Patient 1: 1.97 U mL^{-1}, Patient 6: 2.457 U mL^{-1}, Patient 10: 1.84 U mL^{-1}), the intra-day relative errors range from 5.00% to 7.47%, representing the highest variability observed in the dataset. This concentration-dependent error pattern is characteristic of analytical methods approaching their quantification limits, where signal-to-noise ratios become critical factors in measurement precision. Despite these higher relative errors at low concentrations, the absolute errors remain clinically insignificant, and the confidence limits (±0.09 to ±0.10) demonstrate acceptable measurement uncertainty for diagnostic applications as shown in Table 4.

In contrast, samples with moderate to high CA15-3 concentrations (Patient 2: 183.43 U mL^{-1}, Patient 5: 491.4 U mL^{-1}) exhibit remarkably low relative errors (1.16% and 1.50%, respectively), accompanied by exceptionally tight confidence limits (±0.01 and ±0.14). This superior performance at higher concentrations reflects the optimal operating range of the biosensor, where the Stern–Volmer quenching mechanism

Table 5 The detection of cancer biomarkers by MOF-based optical biosensor[a]

Modified surface	Object	Linear range (ng mL^{-1})	LOD (ng mL^{-1})	Ref.
UiO-66(Fe/Zr)	HeLa cell	103–104 cells per mL	481 cells per mL	41
La(III)-MOF	miRNA-155	2.70 fM–0.01 pM	5.20 fM	42
PDA*/DOX/ZIF-8	miRNA-122	0.02–3.0 nM	12.5 pM	43
drDNA*-BUT-88	miRNA-21 MUC-1*	0.2–1.0 nM 20–100 nM	0.13 nM 4.50 nM	44
MIL-125-NH$_2$	CEA	0.1–200	0.041	45
ZnO nanorod/ZIF-8	CEA	1×10^{-5}–1×10^{-1} U mL^{-1}	1×10^{-5} U mL^{-1}	46
PHMPF*	CA 15-3	2.56×10^{-5}–1.28×10^{-3} U mL^{-1}	2.56×10^{-5} U mL^{-1}	47
Ag@Zn-salen MOF nanocomposite	CA15-3	1.0 to 500 U mL^{-1}	0.12 U mL^{-1}	Current study

[a] PDA, polydopamine; drDNA, DNA-functionalized fluorescent nano probe; MIL, Materials of Institute Lavoisier frameworks; MUC-1, transmembrane glycoprotein mucin-1; PHMPF, prismatic hollow metal-polydopamine framework.

operates most efficiently and signal-to-noise ratios are maximized.

The inter-day precision analysis reveals a systematic increase in variability compared to intra-day measurements, which is expected due to day-to-day variations in environmental conditions, reagent batches, and instrumental parameters. However, the inter-day relative standard deviation (% RSD) values, ranging from 0.02% to 3.53%, remain within acceptable analytical limits established for clinical biomarker assays. Notably, Patient 2 and Patient 9 demonstrate exceptional inter-day precision (0.02% and 0.09% RSD, respectively), indicating remarkable method robustness at their respective concentration levels. The comparative analysis between the proposed biosensor method and the established standard method reveals excellent correlation across the entire concentration range studied, Table 5.

The fact that confidence intervals for the biosensor method overlap with or closely approximate the standard method values for all samples provides strong evidence for analytical equivalence. This concordance is particularly significant for samples spanning three orders of magnitude in concentration (from ~2 U mL^{-1} to ~500 U mL^{-1}), demonstrating the biosensor approach's wide dynamic range and accuracy.

6. Conclusions

This study demonstrates the successful development and validation of a novel Ag@Zn-SalenMOF-based biosensor for highly sensitive and specific detection of CA15-3. The exceptional analytical performance, characterized by a detection limit of 0.12 U mL^{-1}, wide linear range, and excellent precision and accuracy, establishes this biosensor as a superior alternative to conventional immunoassays for CA15-3 detection.

The clinical validation results, showing 93.33% sensitivity and 91.6% specificity, confirm the diagnostic utility of the biosensor for distinguishing between healthy individuals and breast cancer patients. The excellent agreement with reference methods validates the accuracy and reliability of the biosensor for clinical applications.

The remarkable 2-month stability, combined with the robustness and ruggedness of the analytical method, demonstrates the practical viability of this biosensor system for routine clinical implementation. These characteristics address key limitations of existing biosensor technologies and provide a foundation for the widespread clinical adoption of these technologies.

The cost-effectiveness, simplicity of operation, and minimal instrumentation requirements make this biosensor accessible to diverse clinical settings, potentially expanding access to high-quality CA15-3 testing. The democratization of advanced analytical capabilities could significantly impact patient care, particularly in resource-limited environments where sophisticated laboratory infrastructure is unavailable.

The successful development of this biosensor system represents a significant advancement in cancer biomarker detection technology. It offers enhanced analytical performance while addressing practical considerations essential for clinical implementation. The combination of scientific excellence and practical utility positions this biosensor as a valuable addition to the clinical diagnostic toolkit for breast cancer management.

Conflicts of interest

There are no conflicts to declare.

Data availability

All data reported in this paper will be shared by the lead contact upon request. This paper does not report original code. Any additional information required to reanalyze the data reported in this paper is available from the lead contact upon request.

Supplementary information is available. See DOI: **https://doi.org/10.1039/d5ra04548g**.

References

1 M. J. Duffy, N. Harbeck, M. Nap, R. Molina and A. Nicolini, *Eur. J. Cancer*, 2020, **75**, 284–298.
2 F. Lumachi, S. M. Basso and A. A. Brandes, *Expert Rev. Anticancer Ther.*, 2019, **19**, 263–271.
3 C. M. Sturgeon, M. J. Duffy, U. H. Stenman, H. Lilja and N. Brünner, *Clin. Chem.*, 2018, **54**, e11–e79.
4 H. Sung, J. Ferlay, R. L. Siegel, M. Laversanne, I. Soerjomataram and A. Jemal, *CA Cancer J. Clin.*, 2021, **71**, 209–249.
5 H. A. AlGhamdi, Y. M. AlZahrani, S. Alharthi, S. A. Mahmoud and M. S. Attia, *RSC Adv.*, 2023, **13**, 21769–21780.
6 M. S. Attia, A. O. Youssef, M. Gomaa and T. Ibrahim, *Egypt. J. Chem.*, 2021, **64**, 3541–3546.
7 B. Li, H. M. Wen, Y. Cui, W. Zhou and G. Qian, *Adv. Mater.*, 2016, **28**, 8819–8860.
8 L. Jiao, J. Y. R. Seow, W. S. Skinner, Z. U. Wang and H.-L. Jiang, *Mater. Today*, 2019, **27**, 43–68.
9 A. K. Asatkar, M. Tripathi and D. Asatkar, in *Stability and Applications of Coordination Compounds*, IntechOpen, London, UK, 2020, pp. 99–116.
10 W. Zhou, W. Q. Deng and X. Lu, *Interdiscip. Mater.*, 2024, **3**, 87–112.
11 S. J. Wezenberg and A. W. Kleij, *Angew. Chem., Int. Ed.*, 2008, **47**, 2354–2364.
12 H. Zhang, L. L. Lou, K. Yu and S. Liu, *Small*, 2021, **17**, 2005686.
13 Y. Wang, M. Zhang, Z. Yan, S. Ji, S. Xiao and J. Gao, *Theranostics*, 2024, **14**, 1534.
14 P. V. Mane, R. M. Rego, P. L. Yap, D. Losic and M. D. Kurkuri, *Prog. Mater. Sci.*, 2024, 101314.
15 H. Zhang, J. Han and B. Yang, *Adv. Funct. Mater.*, 2010, **20**, 1533–1550.
16 C. M. Doherty, D. Buso, A. J. Hill, S. Furukawa, S. Kitagawa and P. Falcaro, *Acc. Chem. Res.*, 2014, **47**, 396–405.
17 B. Li, J. G. Ma and P. Cheng, *Small*, 2019, **15**, 1804849.
18 A. Hayat, S. Rauf, B. Al Alwan, *et al.*, *Mater. Today Energy*, 2024, 101542.

19 J. Annamalai, P. Murugan, D. Ganapathy, *et al.*, *Chemosphere*, 2022, **298**, 134184.
20 W. Shi, S. Song and H. Zhang, *Chem. Soc. Rev.*, 2013, **42**, 5714–5743.
21 M. Yoshimura and K. Byrappa, *J. Mater. Sci.*, 2008, **43**, 2085–2103.
22 D. Roy, P. Kumar, A. Soni and M. Nemiwal, *Tetrahedron*, 2023, **138**, 133408.
23 P. Tyagi, D. Singh, N. Malik, S. Kumar and R. S. Malik, *Mater. Today*, 2023, **65**, 133–165.
24 Y.-S. Wei, M. Zhang, R. Zou and Q. Xu, *Chem. Rev.*, 2020, **120**, 12089–12174.
25 M. Y. Masoomi, A. Morsali, A. Dhakshinamoorthy and H. Garcia, *Angew. Chem.*, 2019, **131**, 15330–15347.
26 A. Kumari, S. Kaushal and P. P. Singh, *Mater. Today Energy*, 2021, **20**, 100667.
27 M. D. Makhafola, S. A. Balogun and K. D. Modibane, *Energies*, 2024, **17**, 1646.
28 C. S. Silva, N. T. Gomes De Paula and A. P. S. Paim, Application of Metal–Organic Framework Nanocomposites, *Metal–Organic Frameworks in Analytical Chemistry*, RSC, 2023, pp. 415–453.
29 A. L. T. Zheng, E. Y. L. Teo, S. Seenivasagam, *et al.*, *J. Porous Mater.*, 2024, **31**, 1557–1575.
30 J. Dong, X. Han, Y. Liu, H. Li and Y. Cui, *Angew. Chem., Int. Ed.*, 2020, **59**, 13722–13733.
31 U. Karatayeva, S. A. Al Siyabi, B. Brahma Narzary, B. C. Baker and C. F. Faul, *Adv. Sci.*, 2024, **11**, 2308228.
32 S. M. Sheta, S. M. El-Sheikh, M. M. Abd-Elzaher, *et al.*, *Appl. Organomet. Chem.*, 2019, **33**, e5249.
33 S. Yadav, S. P. N. Bukke, S. Prajapati, A. P. Singh, A. K. Chettupalli and B. Nicholas, *Digit. Health*, 2025, **11**, 20552076251342457.
34 E. Dezhakam, R. F. Vayghan and S. Dehghani, *Sci. Rep.*, 2024, **14**, 29850.
35 M. S. A. Abdel-Mottaleb, M. Saif, M. S. Attia, M. M. Abo-Aly and S. N. Mobarez, *Photochem. Photobiol. Sci.*, 2018, **17**, 221–230.
36 M. N. Abou-Omar, M. S. Attia, H. G. Afify, M. A. Amin, R. Boukherroub and E. H. Mohamed, *ACS Omega*, 2021, **6**, 20812–20821.
37 S. Hutapea, M. Elveny, M. A. Amin, M. S. Attia, A. Khan and S. M. Sarkar, *Arabian J. Chem.*, 2021, **14**, 103382.
38 A. A. Elabd and M. S. Attia, *Luminescence*, 2016, **169**, 313–318.
39 M. S. Attia, A. M. Othman, A. O. Youssef and E. El-Raghi, *Luminescence*, 2012, **132**, 2049–2053.
40 M. S. Attia, *Spectrochim. Acta, Part A*, 2009, **74**, 972–976.
41 Y. Zhu, *et al.*, A Single Aptamer-Dependent Sandwich-Type Biosensor for the Colorimetric Detection of Cancer Cells via Direct Coordinately Binding of Bare Bimetallic Metal–Organic Framework-Based Nanozymes, *Biosensors*, 2023, **13**(2), 225.
42 A. Afzalinia and M. Mirzaee, Ultrasensitive fluorescent miRNA biosensor based on a "sandwich" oligonucleotide hybridization and fluorescence resonance energy transfer process using an Ln (III)-MOF and Ag nanoparticles for early cancer diagnosis: application of central composite design, *ACS Appl. Mater. Interfaces*, 2020, **12**(14), 16076–16087.
43 K. Tang, *et al.*, Multifunctional nano-biosensor based on metal-organic framework for enhanced fluorescence imaging of intracellular miRNA-122 and synergistic chemophotothermal therapy of tumor cells, *Anal. Chim. Acta*, 2021, **1176**, 338779.
44 X.-J. Kong, *et al.*, A green-emission metal–organic framework-based nanoprobe for imaging dual tumor biomarkers in living cells, *ACS Appl. Mater. Interfaces*, 2020, **12**(31), 35375–35384.
45 S. Lv, *et al.*, Wet NH3-triggered NH2-MIL-125 (Ti) structural switch for visible fluorescence immunoassay impregnated on paper, *Anal. Chem.*, 2018, **90**(24), 14121–14125.
46 D. Zhao, *et al.*, Highly sensitive microfluidic detection of carcinoembryonic antigen via a synergetic fluorescence enhancement strategy based on the micro/nanostructure optimization of ZnO nanorod arrays and in situ ZIF-8 coating, *Chem. Eng. J.*, 2020, **383**, 123230.
47 Y. Wu, *et al.*, A fluorescent biosensor based on prismatic hollow Metal-polydopamine frameworks and 6-carboxyfluorescein (FAM)-labeled protein aptamer for CA15-3 detection, *Sens. Actuators, B*, 2021, **329**, 129249.